Synthesis of α-Cobalt Hydroxides with Different Intercalated Anions and Effects of Intercalated Anions on Their Morphology, Basal Plane Spacing, and Capacitive Property

Zhong-Ai Hu,* Yu-Long Xie, Yao-Xian Wang, Li-Jing Xie, Guo-Rui Fu, Xiao-Qing Jin, Zi-Yu Zhang, Yu-Ying Yang, and Hong-Ying Wu

Key Laboratory of Polymer, College of Chemistry and Chemical Engineering, Northwest Normal University, Lanzhou 730070, People's Republic of China

Received: December 04, 2008; Revised Manuscript Received: March 19, 2009

The four α-cobalt hydroxides (green or blue) with different intercalated anions were synthesized by a chemical precipitation route in which polyethylene glycol was used as the structure-directing reagent for application in the electrode materials of electrochemical capacitors. Every one among the four samples displays an interesting and distinctive morphology although the synthesis conditions were the same except for the anions. The intercalated anions have a critical effect on the basal plane spacing, morphologies, and capacitive properties of the products. Structural and morphological characterizations were performed by using power X-ray diffraction (XRD) and field emission scanning electron microscopy (FESEM). The component and thermal stability of the sample were respectively measured by FT-IR and thermal analyses, including thermogravimetry (TG) and differential thermogravimetry (DTG). The electrochemical behaviors were measured by cyclic voltammogram and galvanostatic charge−discharge. The specific capacitance is up to 697 F g^{-1} at a charge−discharge current density of 1 A g^{-1} for the sample with intercalated chlorine. But the sample with intercalated sulfate, which has small crystalline size, more disordered structure, and almost perfect alveolate nanostructure with a large surface area, exhibits relatively poor specific capacitance (420 F g^{-1}). The exceptive phenomena caused by intercalated anions were explained by hydrogen bonding and electrostatic forces. Moreover, the relationships between the specific capacitance, basal plane spacing, as well as the content of the interlayer water were discussed in detail for the four as-synthesized samples.

Introduction

Electrochemical capacitors have raised considerable attention over the past decade because of their higher power density and longer cycle life than secondary batteries and their higher energy density compared to conventional electrical double-layer capacitors. Therefore, they are expected to be an attractive replacement for batteries in all-electric cars and plug-in hybrids, as they are quick charging, exhibit temperature stability, and have safety properties suitable to such applications.[1−3] On the basis of their charge-storage mechanisms, supercapacitors can be classified into two types. One is the electric double-layer capacitor, and the other is the redox capacitor. In the former, energy storage arises mainly from the separation of electronic and ionic charges at the interface between electrode materials with high specific area (such as carbon) and the electrolyte solution. In the latter, fast Faradaic reactions take place at the electrode materials at characteristic potentials, as in batteries.[4] Metallic oxides have generally been adopted as electrode materials for pseudocapacitors because of their large capacitance and fast redox kinetics.[5,6] Among the transition metal oxides, hydrous ruthenium dioxide has been recognized as one of the most promising candidates for electrode materials in electrochemical capacitors, as it can store charges reversibly by redox reaction.[7] However, alternatives are being sought to reduce the cost factor and enhance the performance.

Recently, $Co(OH)_2$ materials have been attractive in view of their layered structure with large interlayer spacing, their well-defined electrochemical redox activity, and the possibility of enhanced performance through different preparative methods.[8−15] Hydroxides of cobalt are well-known to crystallize in two polymorphs, α and β.[16,17] The β-form is a stoichiometric phase of the composition $Co(OH)_2$ with brucite-like structure and consists of a hexagonal packing of hydroxyl ions with Co(II) occupying alternate rows of octahedral sites,[18,19] while the α-hydroxides are reported to be isostructural with hydrotalcite-like compounds that consist of positively charged $Co(OH)_{2-x}$ layers and charge balancing anions (e.g., NO_3^-, CO_3^{2-}, Cl^-, etc.) in the interlayer gallery.[20−25] The α-cobalt hydroxide is theoretically expected to exhibit superior electrochemical activity as compared to its β-counterpart because of its poorly or turbostratically crystallized structure. This actually triggered the recent interest in the chemical or electrochemical synthesis and the exact crystal analysis of α-cobalt hydroxide.[26−30] On the other hand, the α-hydroxide intercalated organic anions show long-range magnetic ordering and are regarded as new candidates for organic magnetic materials.[31,32] At the same time, some have reported on the synthesis of cobalt basic salts with different forms.[33,34]

It has been identified that electrochemical behaviors of cobalt hydroxide markedly depend on its grain size, morphology, and crystal structure. So researchers pay great attention to the above three aspects, especially morphology controlled by using various strategies.[35,36] However, other factors, for example, the actions of the intercalated anion in cobalt hydroxide, seem to be ignored generally or have been shown no concern yet. Actually, the pseudocapacitance, which originates from the redox reaction of the electroactive materials, is relative to proton transfer. The intercalated anion will affect the transfer rate of proton through

* To whom correspondence should be addressed. Phone: +86 931 7973255. Fax: +86 931 8859764. E-mail: zhongai@nwnu.edu.cn.

10.1021/jp8106809 CCC: $40.75
Published on Web 06/18/2009

interaction between species, such as hydrogen bonding and electrostatic forces. In the present work, the four α-cobalt hydroxides with different intercalated anions were synthesized by a chemical precipitation route in which polyethylene glycol was used as the structure-directing reagent for application in the electrode materials of electrochemical capacitors. We systematically investigate the effect of the intercalated anion on the basal plane spacing, morphology, content of interlayer water, and capacitive property of the products. To our great surprise, the sample with intercalated sulfate, which has a small crystalline size, more disordered structure, and almost perfect alveolate nanostructure with a large surface area, exhibits relatively poor specific capacitance in comparison with the others, in opposition to what is expected. This suggests quite strongly that there is a scientific requirement to explore inherent factors associated with it.

Experimental Section

Reagents were all of AR grade. Water used in the synthesis and washing was deionized. The α-$Co(OH)_2$ was prepared as follows: the $CoCl_2 \cdot 6H_2O$ (0.01 mol), $Co(NO_3)_2 \cdot 6H_2O$ (0.01 mol), $CoSO_4 \cdot 7H_2O$ (0.01 mol), and $Co(CH_3COO)_2 \cdot 4H_2O$ (0.01 mol) were dissolved in 50 mL of distilled water, respectively, and then 10 g of polyethylene glycol was added to the solution under vigorous stirring, respectively. The aqueous solution of $NH_3 \cdot H_2O$ (25−28%) was dropwise added into the above solution with continuous stirring until the pH of the solution reached 9. After aging for 12 h, the resulting product was separated by suction filtration and rinsed with distilled water and ethanol several times, and then dried at 60 °C for 12 h under vacuum. The four cobalt hydroxides with different intercalated anions (Cl^-, NO_3^-, CH_3COO^-, and SO_4^{2-}) were finally obtained.

The morphology of products was observed by a FESEM (JSM-6701F, Japan). The structure of the cobalt hydroxide was examined by X-ray diffraction (XRD) (D/Max-2400) with Cu Kα radiation ($\lambda = 1.5418$ Å) operating at 40 kV, 60 mA. The components of materials were measured by a Nicolet Nexus 670 FT-IR instrument. Thermal analyses, including thermogravimetry and differential thermal analysis, were carried out with a Perkin-Elmer TG/DTA-6300 instrument in the temperature range of 25−700 °C. A heating rate of 10 deg min^{-1} in nitrogen with a flow rate of 20 mL min^{-1} was used.

The working electrodes were prepared by pressing mixtures of the as-prepared samples, acetylene black, conducting graphite, and polytetrafluoroethylene (PTFE) binder (weight ratio of 75:10:10:5) onto a nickel foam current collector. A typical three-electrode experimental cell equipped with a working electrode, a platinum foil counter electrode, and a Hg/HgO reference electrode was used for measuring the electrochemical properties of the working electrode and its performance as a faradaic supercapacitor. All electrochemical measurements were carried out in 6 mol/L of aqueous KOH solution as electrolyte. Cyclic voltammetry (CV) and galvanostatic charge−discharge were carried out on a CHI660B electrochemical working station (CH Instrument) and cyclic stability of the four electrodes was evaluated with a LAND CT2001A multichannel galvanostat in the potential range of 0 to 0.5 V (vs. Hg/HgO).

All solutions used in this work were prepared with double-distilled water. All electrochemical experiments were carried out at room temperature and the potentials were referenced to Hg/HgO.

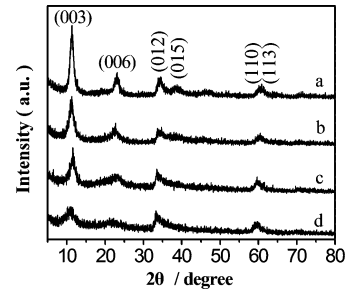

Figure 1. XRD patterns of α-cobalt hydroxide samples with intercalated chloride (a), nitrate (b), acetate (c), and sulfate (d) anions.

Results and Discussion

XRD Characterization. Among the as-synthesized products, three samples containing intercalated anion Cl^-, NO_3^-, or CH_3COO^- are green, while the sample containing intercalated anion SO_4^{2-} is blue. Figure 1 shows XRD patterns of four samples. The third diffraction peak has the typical broad "sawtooth" shape, with a sharp rise at the low-angle side and pronounced asymmetry on the high-angle side, indicating that layer stacking in the as-synthesized samples must be rather loose and defective, leading to a turbostratic structure. It is identified that the main difference between the α phase and the β phase for $Co(OH)_2$ resides in the stacking of the layers along the *C*-axis. β-$Co(OH)_2$ layers are perfectly stacked along the *C*-axis with an interlamellar distance of 4.6 Å,[37] without any intercalated species, but α-$Co(OH)_2$ layers are randomly oriented and separated by intercalated water molecules bonded to the hydroxyl groups by hydrogen bonds. Therefore, four samples show certain α phase characteristics. Nevertheless, there is a slight different in intensity, position, and shape of diffraction peaks and basal plane spacing. All the samples have large basal plane spacing, but the values of the basal plane spacing depend on the intercalated anion. In the order of intercalated anions Cl^-, NO_3^-, CH_3COO^-, and SO_4^{2-}, the corresponding spacing is 7.797, 7.852, 7.902, and 8.155 Å, respectively, which is consistent with the anionic radii. Except for the sample with intercalated chlorine, the others represent a slight expansion in interlayer spacing. In practice, the lattice parameter *a* corresponds to the average cation−cation distance within a given layer, while parameter *c* corresponds to several times the thickness of an elemental "sandwich". The first parameter depends mostly on the ionic radii of the layer cations, while the second one depends on the size of the intercalated anion and on its orientation in the interlayer (in the case of nonspherical anions), as well as on the electrostatic interaction between the interlayer species and the layers. Furthermore, the diffractograms clearly suggest that the compound containing intercalated anion Cl^-, showing relatively sharp *hkl* reflection peaks, has a higher crystalline nature than the other product giving an XRD spectra signal/noise ratio relatively high. Among the four samples, the compound containing intercalated anion SO_4^{2-} displays the lowest crystallinity and smallest crystallite sizes revealed by a considerable broadening of the peaks in the diffraction pattern due to some disorder of the layers oriented along the *c*-axis leading to a small number of parallel planes available for the diffraction.

FT-IR Measurement. The FT-IR spectra of the compounds are shown in Figure 2. The infrared absorptions (curve e) of β-$Co(OH)_2$ without any additional intercalated anions was given for comparison and discussion. These spectra exhibit broad and intense bands centered around 3400 cm^{-1} corresponding to the O−H stretching vibrations of the interlayer water molecules and

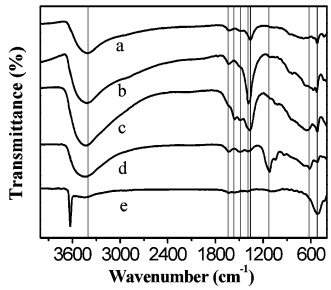

Figure 2. The FT-IR spectra of α-cobalt hydroxide samples with intercalated chloride (a), nitrate (b), acetate (c), sulfate (d) anions, and β-cobalt hydroxide sample (e).

hydrogen atoms bound to OH groups. But the sharp peak, as shown by curve e in Figure 2, attributed to the O−H stretching mode of the free Co−OH groups, disappears due to due to the existence of hydrogen bonding between the hydrogen atoms and the intercalated anions or water molecules within the layers. The bands appearing around 1634 cm^{-1} correspond to the water molecules deformation vibration. Peaks around 1466 cm^{-1} are assigned to carbonate ions, and their existence could be due to the dissolution of carbon dioxide molecules in water. The other absorption band associated with carbonate ions was too weak to be identifiable, implying a low content of carbonate ions. In the low wavenumber region below 800 cm^{-1}, the absorptions are associated with Co−O stretching and Co−OH bending vibrations.[22] The band at about 663 cm^{-1} can be assigned to the δ (Co−O−H). The absorption band at about 528 cm^{-1} can be assigned to the υ(Co−O) stretching vibrations. Curve a suggests apparently that the predominant anionic species in the interlayer of the α-$Co(OH)_2$ sample is Cl^- ions, which were accommodated in the interlayer space together with water molecules and CO_3^{2-} ions. Besides, the characteristic absorption peaks of the intercalated anion can be observed in the figure. Curve b shows a sharp peak at 1380 cm^{-1} because of the intercalated nitrate, and curve c shows two peaks due to the carbonyl group symmetric and asymmetric stretching vibrations at 1370 and 1490 cm^{-1}, respectively. The single intense absorption associated with sulfate appears at 1120 cm^{-1} with a shoulder at 1045 cm^{-1} as shown by curve d. Furthermore, the absorption peaks of the O−H stretching vibrations for five samples (from curves a to e) appear respectively at 3414, 3419, 3431, 3440, and 3630 cm^{-1}, which show a blue-shift. The O−H stretch for β-$Co(OH)_2$ was found at the highest frequency indicative of very weak or absent true hydrogen bonding. In comparison with β-$Co(OH)_2$, the O−H stretching vibration frequency of the four as-prepared samples is much lower, implying the existence of hydrogen bonding. It could be concluded that hydrogen bonding is stronger in the case of intercalated anion Cl^- but weaker in the case of intercalated anion SO_4^{2-}.

TG-DTG Analysis. The hydroxyl vacancies would then be occupied by water molecules to yield slabs of composition $[Co(OH)_{2-x}(H_2O)_x]^{x+}$. This so-called structural water would be a fraction of the total water content, which includes the adsorbed and intercalated water molecules as well.[38] The dehydration is expected to be a multistep process, with the adsorbed and intercalated water loss occurring below the decomposition temperature and the structural water loss taking place along with the dehydroxylation−deanation of the hydroxide during the decomposition step. In the case of the sample with intercalated chlorine (see Figure 3a) reported here the adsorbed and intercalated water species are lost in a single broad step in the range 25−152 °C, while decomposition begins at 175 °C. Most of the weight loss ends at 248 °C, but an extended flanking loss is seen up to 306 °C. The weight loss (9.9%) between 50 and 152 °C is assigned to the evaporation of the intercalated water molecules. The range from 152 to 306 °C is associated with the loss of water produced by dehydroxylation of the hydroxide layers combined with the partial loss of the anionic species (CO_3^{2-} and Cl^-). In the case of the sample with intercalated nitrate (Figure 3b) the weight loss (8.9%) between 50 and 151 °C is assigned to the evaporation of the intercalated water molecules. The range from 151 to 278 °C is associated with the loss of water produced by dehydroxylation of the hydroxide layers combined with the partial loss of the anionic species (CO_3^{2-} and NO_3^-). In the case of the sample with intercalated acetate (Figure 3c) the weight loss (7.2%) between 50 and 160 °C is assigned to the evaporation of the intercalated water molecules. The range from 160 to 350 °C is associated with the loss of water produced by dehydroxylation of the hydroxide layers combined with the loss of the anionic species (CO_3^{2-} and CH_3COO^-). Similarly, in the case of the sample with intercalated sulfate (Figure 3d) the weight loss (6.4%) between 50 and 153 °C is assigned to the evaporation of the intercalated water molecules. The range from 153 to 347 °C is associated with the loss of water produced by dehydroxylation of the hydroxide layers combined with the loss of the anionic species (CO_3^{2-}). Finally, the ending at about 700 °C can be attributed to the loss of the interlayer SO_4^{2-} anion. We can conclude from TG analysis that the content of the intercalated water is relative to the interlayer spacing or the radii of the intercalated anion. In brief, the content of structural water decreases with the order of intercalated anion Cl^-, NO_3^-, CH_3COO^-, and SO_4^{2-}, which is consistent with the size of anions. The larger size of the intercalated anion may occupy the intercalated water vacancies. A similar feature observed in the TG of α-cobalt hydroxide has been attributed to the loss of structural water and anions from the micropores of the crumbling sheets of the product of decomposition.[39]

FESEM Images. The surface morphologies of the as-synthesized samples with intercalated anion chloride (photograph a), nitrate (photograph b), acetate (photograph c), and sulfate (photograph d) are imaged by FESEM, as shown in Figure 4. It can be seen from Figure 4a that cobalt hydroxides, in the case of intercalated anion Cl^-, exhibit binary morphology that are comprise of sheets and clusters assembled by solid rods The sheets are about 30 nm in average thickness and more than 1 μm in average size, while the nanorods are about 30 nm in diameter and 100−300 nm in length. The FESEM image of the sample with intercalated nitrate is shown in Figure 4b. A cluster with microstructure is observed clearly. We call it a thin-walled cell configuration, in which small sheets, acting as a wall, joined large sheets to form various cells. It is found from the photograph that sheets are uniform in thickness with an average value of ∼10 nm. Figure 4c shows a flowerlike architecture in the case of interlayer acetate, which consists of nanostructured curly lamina. The flowerlike architecture is 2−3 μm in diameter and the curly lamina is about 10 nm in thickness. Figure 4d displays porous nanostructures in the case of interlayer sulfate (blue sample), which reveal an almost perfect alveolate nano-cluster. The diameters of alveolate clusters are in the ranges of 200−300 nm. Furthermore, every alveolate cluster is comprised of many microsheets with a thickness of 10 nm. This special configuration could result from the self-assembly by driving of panel Gibb's energy. Among four samples, the cobalt hydroxide with interlayer sulfate seems to provide the highest interfacial area of solid/liquid reaction. In conclusion, the architecture

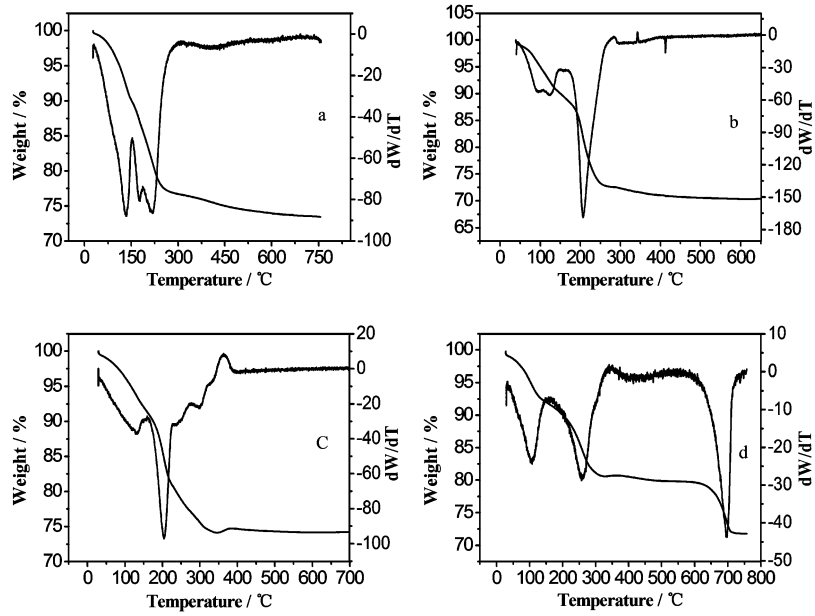

Figure 3. TG-DTG of α-cobalt hydroxide samples with intercalated chloride (a), nitrate (b), acetate (c), and sulfate (d) anions.

element of the sample is sheet or layer due to template action of polyethylene glycol, but the intercalated anions lead to quite distinctive morphology. The different intercalated anions provide a different located force field, resulting in a special growth of the materials.

Electrochemical Properties. Cyclic voltammetry (CV) is considered to be a suitable tool to indicate the capacitive behavior of any material. Figure 5 shows the CV curves of the samples with intercalated different anions in 6 M KOH electrolyte at a scan rate of 5 mV s^{-1}. As shown in Figure 5, there are two redox peaks due to the following Faradaic reactions of $Co(OH)_2$:

$$Co(OH)_2 + OH^- \leftrightarrow CoOOH + H_2O + e^- \quad (1)$$

$$CoOOH + OH^- \leftrightarrow CoO_2 + H_2O + e^- \quad (2)$$

One quasireversible electron transfer process is visible in every curve, indicating that the measured capacitance is mainly based on redox mechanism.[40] Furthermore, the shape of the curves (Figure 5) revealed that the capacitance characteristic was distinct from that of the electric double layer capacitor, which would produce a CV curve close to an ideal rectangular shape. The integral area is maximal for the sample with the intercalated chlorine, but minimal for the sample with the intercalated sulfate. To expose cyclic voltammetric characteristic of the electrode, the response of the anodic current to sweep rates was measured by taking the compound with the intercalated chlorine as an example. It can be seen from Figure 6 that the anodic peak current i_p vs. $V^{1/2}$ plot, where V is the voltage scan rate, gives a reasonable linear relationship, while i_p vs. V gives a nonlinear relationship. In semi-infinite diffusion controlled cyclic voltammetry in liquid electrolytes, i_p vs. $V^{1/2}$ gives a linear relationship regardless of the scan rate for a kinetically uncomplicated redox reaction; for an adsorption process, i_p vs. V is expected to be linear at different rates. So it can be suggested that the redox reaction of cobalt hydroxide is a diffusion-limited reaction, as noted by other authors.[41−43]

Figure 7 shows discharge curves for $Co(OH)_2$ with different intercalated anion (chloride (curve a), nitrate (curve b), acetate (curve c), and sulfate (curve d)) and the charge−discharge (CD) curves (insert) in the case of intercatalated chloride in 6 M KOH electrolyte at 1 A g^{-1} current density in the potential range of −0.1 to 0.4 V. One can observe redox characteristics in the *CD* curves that are directly related to the redox peaks of $Co(OH)_2$ in the CV curves (Figure 5). The profiles of the CD curves are close to an ideal triangular shape. The specific capacitances, calculated on the base of the discharge curves for the samples with intercalated anion chloride (curve a), nitrate (curve b), acetate (curve c), and sulfate (curve d), are 697, 638, 526, and 420 F g^{-1}, respectively. So far as the cobalt hydroxide synthesized by the chemical route is concerned, all the samples reach high specific capacitances. The spacing, water content, and crystalline defects of α-cobalt hydroxide are responsible for superior supercapacitive properties.

Cyclic stability of the four electrodes is also evaluated by repeating the CV scan for 100 cycles, and Figure 8 displays the specific capacitance (SC) of the α-cobalt hydroxide with different intercalated anion (chloride (curve a), nitrate (curve b), acetate (curve c), and sulfate (curve d)) as a function of charge−discharge cycle numbers at a current density of 3 A g^{-1}. We notice that the repetitive charge/discharge induces degradation of the porous structure, resulting in a noticeable discharge specific capacitance loss (about 27% for intercalated chloride anion, 44% for intercalated nitrate anion, 43% for intercalated acetate anion, and 52% for intercalated sulfate anion). But the specific capacitance loss of the α-cobalt hydroxide with intercalated chloride anion electrode is relatively slighter than that of other electrodes after 100 cycles. Despite the relatively poor electrochemical stability, this is important in searching for maximizing the capacitance and cyclic stability of this sort of material.

Further analysis of the above data leads to several interesting details. For example, there is a notable negative correlation between the value of the specific capacitances and the proton affinity of the intercalated anions. Furthermore, XRD spectra and FESEM images indicate that the sample with intercalated sulfate has a small crystalline size, more disordered structure, and almost perfect alveolate nanostructure with a large surface area, implying that it should have more excellent capacitive properties than the others. To our great surprise, however, this sample has poor specific capacitance, in opposition to what is expected. Moreover, the specific capacitance of the four as-

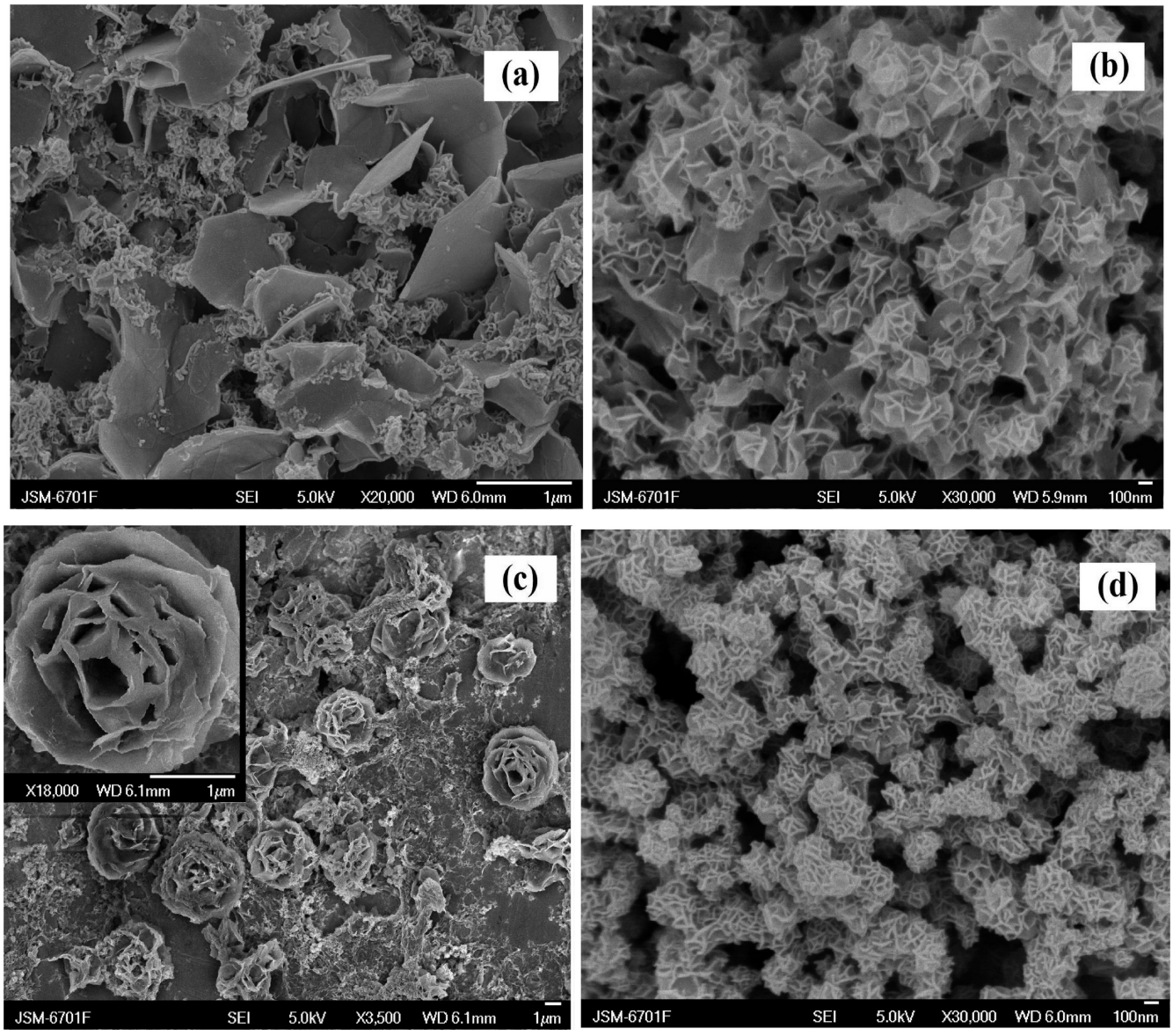

Figure 4. FESEM of α-cobalt hydroxide samples with intercalated chloride (a), nitrate (b), acetate (c), and sulfate (d) anions.

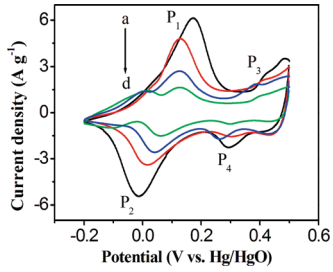

Figure 5. CV curves of α-cobalt hydroxide samples with intercalated chloride (a), nitrate (b), acetate (c), and sulfate (d) anions at 5 mV s^{-1} scan rates within a potential window of −0.2 to 0.5 V vs. Hg/HgO.

synthesized samples decreases with an increase in their spacing. This suggests quite strongly that there is an inherent effect on the capacitive properties of α-cobalt hydroxide. We consider that the hydrogen bonding between the interlayer water molecules and OH groups bound to cobalt ions and the affinity between the intercalated anions and proton plays have an important role in the diffusion rate of the proton, which may be a determining step for redox reaction in the charge−discharge

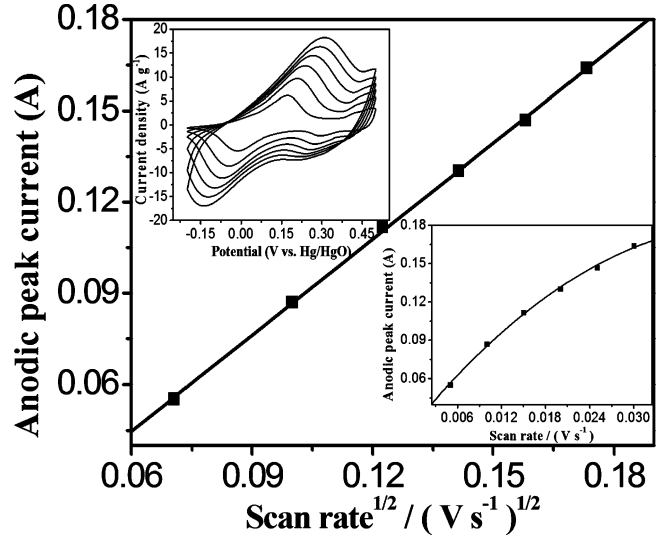

Figure 6. Variation of anodic peak current with scan rate$^{1/2}$ and variation of anodic peak current with scan rate (insert) for α-cobalt hydroxide samples with intercalated chloride anion electrode.

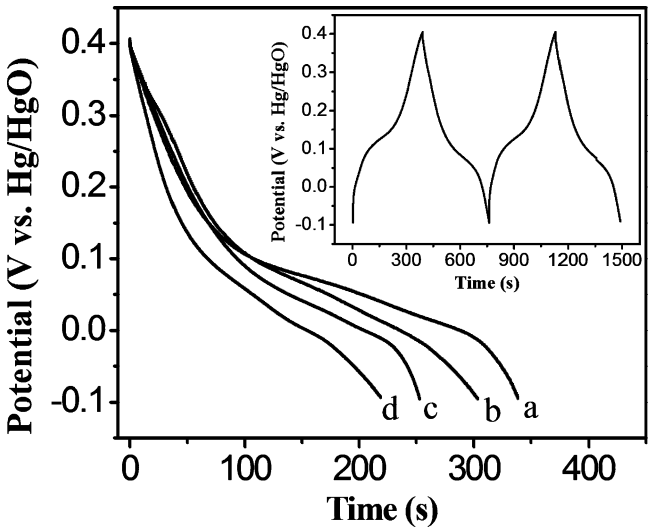

Figure 7. Discharge curves of α-cobalt hydroxide samples with intercalated chloride (a), nitrate (b), acetate (c), and sulfate (d) anions and charge−discharge curves (insert) containing chloride anion in the potential rage from −0.1 to 0.4 V at a current density of 1 A g^{-1}.

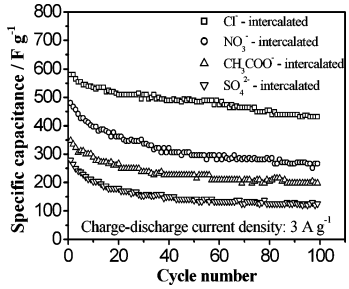

Figure 8. Cycle life data of α-cobalt hydroxide samples with intercalated chloride (a), nitrate (b), acetate (c), and sulfate (d) anions (3 A g^{-1}).

processes. The sufficient hydrogen bonding between the interlayer water molecules and the Co−OH group may be beneficial to mitigating polarization of the electrode or enhancing utilization of the active materials. The TG-DTG analysis shows that the content of the interlayer water decreases with the order of the intercalated anion Cl^-, NO_3^-, CH_3COO^-, and SO_4^{2-}. This change is consistent with the increase of the OH-stretch vibrations as shown in the IR spectra of the samples. The high frequency of the O−H stretching vibrations is indicative of weak hydrogen bonding. In particular, the sulfate ion has a strong polarity and its O atom has a large electronic negativity, and might form a hydrogen bond with the interlayer water at this site, which hinders water molecules intercalated in the layer from forming a hydrogen bond with the Co−OH group. Specially, the acetate ion contains a hydrophobic group, which also hinders water molecules intercalated in the layer from forming a hydrogen bond. The effect of the nitrate ion is similar with sulfate, but weak. However, the chloride ions may be coordinated with Co ions, which might have no effect on the intercalation of water molecules.

Conclusions

The four α-cobalt hydroxides with distinctive morphology were successfully synthesized by using polyethylene glycol as the structure-directing reagent. The intercalated anions had a critical effect on the basal plane spacing, the content of the structural water, morphologies, and capacitive properties of the products. Except for the sample with intercalated chlorine, the others represent a slight expansion in basal plane spacing. The spacing of the cobalt hydroxide with intercalated sulfate is maximal and up to 8.155 Å. The content of structural water decreases with the order of intercalated anion Cl^-, NO_3^-, CH_3COO^-, and SO_4^{2-}, which is negatively consistent with the size of anions. Among the four samples, every one displays an interesting and distinctive morphology. However, the architecture element of the sample is sheet or layer due to the template action of polyethylene glycol. The specific capacitances of the samples with intercalated anion chloride, nitrate, acetate, and sulfate are 697, 638, 526, and 420 F g^{-1}, respectively. There is a notable negative correlation between the value of the specific capacitances and the proton affinity of the intercalated anions. Furthermore, the hydrogen bonding between the interlayer water molecules and OH groups bound to cobalt ions and the affinity between the intercalated anions and proton plays an important role in the diffusion rate of the proton, which directly affects the capacitive properties of α-cobalt hydroxide.

Acknowledgement. .

We gratefully acknowledge the support of this work by Natural Science Funds in Gansu Science and Technology Committee (0803RJA005) and the postgraduate advisor program of Provincial Education Department of Gansu.

References and Notes

(1) Zhao, D. D.; Zhou, W. J.; Li, H. L. *Chem. Mater.* **2007**, *19*, 3882.
(2) Conway, B. E. *Electrochemical Supercapacitors*; Kluwer-Plenum Pub. Co.: New York, 1999.
(3) Zhou, W.-J.; Zhang, J.; Xue, T.; Zhao, D.-D.; Li, H.-L. *J. Mater. Chem.* **2008**, *18*, 905.
(4) Park, J. H.; Ko, J. M.; Park, O. O.; Kim, D.-W. *J. Power Sources* **2002**, *105*, 20.
(5) Miller, J. S. *Adv. Mater.* **1993**, *5*, 587.
(6) Fusalba, F.; Ho, H. A.; Breau, L.; Belanger, D. *Chem. Mater.* **2000**, *12*, 2581.
(7) Ryu, K. S.; Jeong, S. K.; Joo, J.; Kim, K. M. *J. Phys. Chem. B* **2007**, *111*, 731.
(8) Cao, L.; Xu, F.; Liang, Y. Y.; Li, H. L. *Adv. Mater.* **2004**, *16*, 1853.
(9) Gupta, V.; Gupta, S.; Miura, N. *J. Power Sources* **2008**, *177*, 685.
(10) Hu, Z. A.; Mo, L. P.; Feng, X. J.; Shi, J.; Wang, Y. X.; Xie, Y. L. *Mater. Chem. Phys.* **2009**, *114*, 53.
(11) Zhou, W. J.; Zhang, J.; Xue, T.; Zhao, D. D.; Li, H. L. *J. Mater. Chem.* **2008**, *18*, 905.
(12) Gupta, V.; Kusahara, T.; Toyama, H.; Gupta, S.; Miura, N. *Electrochem. Commun.* **2007**, *9*, 2315.
(13) Jayashree, R. S.; Kamath, P. V. *J. Mater. Chem.* **1999**, *9*, 961.
(14) Zhou, W. J.; Zhao, D. D.; Xu, M. W.; Xu, C. L.; Li, H.-L. *Electrochim. Acta* **2008**, *53*, 7210.
(15) Hu, Z. A.; Xie, Y. L.; Wang, Y. X.; Wu, H. Y.; Yang, Y. Y.; Zhang, Z. Y. *Electrochim. Acta* **2009**, *54*, 2737.
(16) Bish, D. L.; Livingstore, A. *Miner. Mag.* **1981**, *44*, 339.
(17) Oliva, P.; Leonardi, J.; Laurent, J. F.; Delmas, C.; Braconnier, J. J.; Figlarz, M.; Fievet, F. *J. Power Sources* **1982**, *8*, 229.
(18) Benson, P.; Briggs, G. W. D.; Wynne-Jones, W. F. K. *Electrochim. Acta* **1964**, *9*, 275.
(19) Mockenhaupt, Ch.; Zeiske, Th.; Lutz, H. D. *J. Mol. Struct.* **1998**, *443*, 191.
(20) Ismail, J.; Ahmed, M. F.; Kamath, P. V. *J. Solid State Chem.* **1995**, *114*, 550.
(21) Dixit, M.; Subbanna, G. N.; Kamath, P. V. *J. Mater. Chem.* **1996**, *6*, 1429.
(22) Xu, Z. P.; Zeng, H. C. *Chem. Mater.* **1999**, *11*, 67.
(23) Jeevanandam, P.; Koltypin, Yu.; Mastai, Y. *J. Mater. Chem.* **2000**, *10*, 511.
(24) Zhu, Y.; Li, H.; Koltypin, Y.; Gedanken, A. *J. Mater. Chem.* **2002**, *12*, 729.
(25) Xu, R.; Zeng, H. C. *J. Phys. Chem. B* **2003**, *107*, 12643.
(26) El-Batlouni, H.; El-Rassy, H.; Al-Ghoul, M. *J. Phys. Chem. A* **2008**, *112*, 7755.
(27) Yarger, M. S.; Steinmiller, E. M. P.; Choi, K.-S. *Chem. Commun.* **2007**, 159.

(28) Ma, R.; Liu, Z.; Takada, K.; Fukuda, K.; Iyi, N.; Bando, Y.; Sasaki, T. *J. Am. Chem. Soc.* **2007**, *129*, 5257.
(29) Du, Y.; O'Hare, D. *Inorg. Chem.* **2008**, *47*, 3234.
(30) Ma, R.; Liu, Z.; Takada, K.; Fukuda, K.; Ebina, Y.; Bando, Y.; Sasaki, T. *Inorg. Chem.* **2006**, *45*, 3964.
(31) Kurmoo, M. *Chem. Mater.* **1999**, *11*, 3370.
(32) Rujiwatra, A.; Kepert, C. J.; Claridge, J. B.; Rosseinsky, M. J.; Kumagai, H.; Kurmoo, M. *J. Am. Chem. Soc.* **2001**, *123*, 10584.
(33) Liu, B. H.; Yu, S. H.; Chen, S. F.; Wu, C. Y. *J. Phys. Chem. B* **2006**, *110*, 4039.
(34) Jeevanandam, P.; Koltypin, Y.; Gedanken, A. *Nano Lett.* **2001**, *1*, 263.
(35) Liu, Z. P.; Ma, R. Z.; Osada, M.; Takada, K.; Sasaki, T. *J. Am. Chem. Soc.* **2005**, *127*, 13869.
(36) Hou, Y.; Kondoh, H.; Shimojo, M.; Kogure, T.; Ohta, T. *J. Phys. Chem. B* **2005**, *109*, 19094.
(37) Zhu, Y.; Li, H.; Koltypin, Y.; Gedanken, A. *J. Mater. Chem.* **2002**, *12*, 729.
(38) Mani, B.; de Neufville, J. P. *J. Electrochem. Soc.* **1988**, *35*, 800.
(39) Delahaye-Vidal, A.; Tekaia-Elhsissen, K.; Genin, P.; Figlarz, M. *Eur. J. Solid State Inorg. Chem.* **1994**, *31*, 823.
(40) KuanXin, H.; Xiaogang, Z.; Juan, L. *Electrochim. Acta* **2006**, *51*, 1289.
(41) Bing, L.; Huatang, Y.; Yunshi, Z.; Zuoxiang, Z.; Deying, S. *J. Power Sources* **1999**, *79*, 277.
(42) MarArthur, D. M. *J. Electrochem. Soc.* **1970**, *117*, 729.
(43) Guzman, R. S. S.; Vilche, J. R.; Arvia, A. J. *J. Electrochem. Soc.* **1978**, *125*, 1578.

JP8106809